Inorganic Chemistry

Article

pubs.acs.org/IC

Cooperative Assembly of Zn Cross-Linked Artificial Tripeptides with Pendant Hydroxyquinoline Ligands

Meng Zhang, Joy A. Gallagher, Matthew B. Coppock, Lisa M. Pantzar, and Mary Elizabeth Williams*

Department of Chemistry, The Pennsylvania State University, 104 Chemistry Building, University Park, Pennsylvania 16802, United States

Supporting Information

ABSTRACT: An artificial peptide with three pendant hydroxyquinoline (hq) ligands on a palindromic backbone was designed and used to form multimetallic assemblies. Reaction of the tripeptide with zinc acetate led to a highly fluorescent tripeptide duplex with three Zn(II) coordinative cross-links. The binding process was monitored using spectrophotometric absorbance and emission titrations; NMR spectroscopy and mass spectrometry confirmed the identity and stoichiometry of the product structure. Titrations monitoring duplex formation of the zinc-tripeptide structure had a sigmoidal shape, equilibrium constant larger than the monomeric analogue, and a Hill coefficient >1, all of which indicate positive cooperativity. Photophysical characterization of the quantum yield, excited state lifetime, and polarization anisotropy are compared with the monometallic zinc-hq analogue. A higher than expected quantum yield for the trimetallic complex suggests a structure in which the central chromophore is shielded from solvent by π-stacking with neighboring Zn(II) complexes.

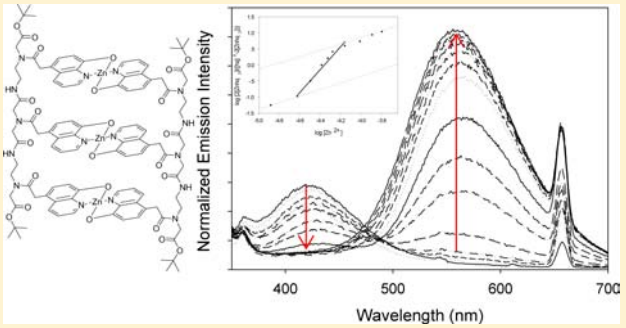

INTRODUCTION

The control of electronic properties in supramolecular systems has acquired growing interest in recent years, since it provides theoretical premises for the design of photonic molecular wires and efficient artificial photosynthetic systems.[1,2] Self-assembly via molecular recognition is a common approach to create such functional supramolecular architectures by often employing metal complexes as necessary components because of their unique optical and electrochemical properties.[3,4a] Among attempts to design photonic wires and mimic processes of photosynthesis, structures relying upon noncovalent interactions between well-arranged chromophores or fluorophores have drawn the most attention.[4] These noncovalently linked molecules enable tunable electron and/or energy flows along the length of the assemblies via *through-space* pathways between electron donors and acceptors.[4,5]

To construct multisite chromophore-acceptor structures, our group has previously employed the aminoethylglycine (aeg) backbone, which is characteristic of peptide nucleic acid (PNA),[6] in conjunction with pendant *N*-heterocyclic ligands to create single-stranded,[7] duplex,[8] and hairpin[9] structures that form upon the addition of transition metal ions. The geometry these complexes form is a result of the denticity of the ligands used, as well as the coordinative saturation of the metal center. In some cases, the metal centers are held within close enough spatial proximity to electronically interact.[8d] Initial work implemented a synthetic strategy involving solution phase peptide chemistry with an incremental lengthening approach that constructed sequences from the N to C terminus.[7a,b,8a] Upon addition of metal ions to these oligopeptides, two different isomers of the duplex can form: antiparallel and parallel conformations. One strategy taken to avoid formation of these isomers is to follow the methodology from dendrimers (building out from the core) and use a divergent approach toward synthesizing symmetrical peptides.[10] This strategy affords a single isomer upon addition of the metal.

Since existing data suggest that the electronic repulsion between charged complexes within our molecules may counteract the structural design responsible for forcing the metal centers within close proximity to one another, we chose the luminescent 8-hydroxyquinoline (hq) ligand to form neutral complexes that have the potential for π-stacking within the structure. Other studies have used hq and its Zn complexes for solid state electroluminescence[11] and has more recently been incorporated in PNA duplexes as an artificial metallobase.[12] Our structures are unique because the only mode for cross-linking two strands to form duplex structures is by metal complexation to the pendant ligands, resulting in multimetallic structures that are charge neutral and highly luminescent.

The inclusion of hq and its zinc complex within our structures make it possible to investigate the electronic communication between metal centers using fluorimetry. When the ligand and metal complex are emissive at different wavelengths, it provides an opportunity to quantitatively measure equilibrium concentrations and obtain an association

Received: February 28, 2012
Published: October 5, 2012

   dx.doi.org/10.1021/ic3004504 | *Inorg. Chem.* 2012, 51, 11315−11323

constant (K_a), which can be extremely difficult in structures with overlapping absorbance transitions. We reasoned that because the hq ligand and [Zn(hq)$_2$] complex are each luminescent at different wavelengths, they could be used as probes to obtain a quantitative measurement of K_a, and examine the role of structure on photophysical properties and binding. We expect to see geometric interactions between metallic ligand centers during the coordination process, such as cooperative behavior observed in the self-assembly of double-helical metal oligo-bpy complexes.[13] It is of particular interest to obtain binding kinetics and relative stabilities of our self-assemblies, which are important to our future design of photonic wires and light-harvesting antennas using these Zn-linked hydroxyquinoline complexes.

The structure of the Zn-linked hydroxyquinoline tripeptide duplex, as shown in Scheme 1, is the target for the synthesis and analysis in this report. Following synthesis of the tripeptide, reaction with Zn(II) is quantitatively analyzed and the structure is confirmed by analysis with UV−visible spectroscopy, emission spectroscopy, and mass spectroscopy. Polarization anisotropy was employed to probe the differences in the size of the Zn(II) cross-linked tripeptide and monomer complexes. In the case of the tripeptide, the data suggest that during formation of the Zn-linked structure, positive cooperativity leads to a large K_a and Hill coefficient. The electronic and geometric interactions within the tripeptide structure are realized by comparing the behavior of the Zn-linked monomer.

Scheme 1. Structure of the Zn-Linked Hydroxyquinoline Tripeptide Duplex

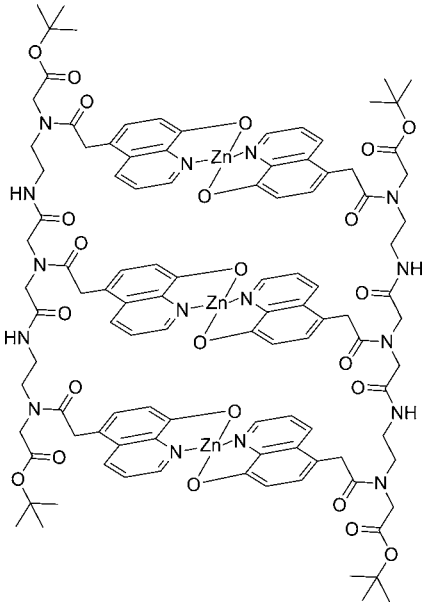

EXPERIMENTAL SECTION

Chemicals and Reagents. *N*-Hydroxybenzotriazole (HOBT), 1-ethyl-3-(3-dimethylaminopropyl)carbodiimide hydrochloride (EDC), and *N*-ethyl diisopropylamine (DIPEA) were purchased from Advanced ChemTech. Zinc(II) acetate (anhydrous, 99.9%) was purchased from Alfa Aesar. All solvents were used as received without further purification unless otherwise noted. The syntheses of 5-(8-hydroxyquinolyl)acetic acid hydrochloride,[14] *tert*-butyl *N*-[2-(*N*-9-fluorenylmethoxycarbonyl)aminoethyl] glycinate hydrochloride (Fmoc-aeg-O*t*Bu·HCl),[15] and diethyl iminodiacetate[16] were performed and the products characterized as previously reported.

SYNTHESES

Ethyl [*N*-5-(8-Hydroxyquinoline)-acetyl] Iminodiacetate (1). 5-(8-Hydroxyquinolyl)acetic acid hydrochloride (2.3 g, 9.8 mmol), EDC (1.9 g, 9.8 mmol), HOBT (1.3 g, 9.8 mmol) were added to 150 mL of dry dichloromethane and stirred in an ice bath under nitrogen for 15 min. DIPEA (3.4 mL, 20 mmol) was added and the yellow solution was stirred for another 45 min. Diethyl iminodiacetate (0.93 g, 4.9 mmol) in 30 mL of dry dichloromethane was added (4.9 mmol), and the solution was stirred for 48 h at room temperature. The reaction mixture was washed with water (3 × 50 mL). The organic layer was dried over sodium sulfate and the solvent removed under vacuum. The crude product was purified using silica column chromatography with a 5% methanol in dichloromethane mobile phase; like fractions were combined, and the solvent was evaporated to yield a pale yellow oil (1.0 g, 75%). (ESI+) MS calculated: $[M+H]^+$ = 375.2; found $[M+H]^+$ = 375.3. ^{1}H NMR (400 MHz, $CDCl_3$): δ = 1.10 (m, 6H), 2.00 (s, 1H), 3.23 (s, 2H), 3.80−4.10 (m, 8H), 6.88 (d, J = 8 Hz, 1H), 7.10 (d, J = 8 Hz, 1H), 7.17 (q, J_1 = 12 Hz, J_2 = 4 Hz, 1H), 8.05 (d, J = 12 Hz, 1H), 8.52 (d, J = 4 Hz, 1H) ppm.

[*N*-5-(8-Hydroxyquinoline)-acetyl] Iminodiacetic Acid (2). Compound **1** (1.0 g, 3.6 mmol) was dissolved in 20 mL of tetrahydrofuran and 6.2 mL of 2 M sodium hydroxide was added dropwise. The reaction mixture was stirred overnight. Water (10 mL) was added, and the mixture was washed with DCM (3 × 15 mL). The aqueous layer was acidified using 1 M hydrochloric acid while cooling in an ice bath until a pH of 7 was reached, and the solvent was removed by vacuum to yield an orange solid (0.86 g, 74%). (ESI+) MS calculated: $[M+H]^+$ = 319.1; found $[M+H]^+$ = 319.2. ^{1}H NMR (400 MHz, CD_3OD): δ = 3.48 (s, 2H), 3.97−4.15 (m, 4H), 7.06 (d, J = 6 Hz, 1H), 7.25 (d, J = 6 Hz, 1H), 7.43 (q, J_1 = 9 Hz, J_2 = 6 Hz, 1H), 8.45 (d, J = 9 Hz, 1H), 8.77 (d, J = 6 Hz, 1H) ppm.

***Tert*-butyl{*N*-[2-(*N*-9-Fluorenylmethyoxycarbonylamino)ethyl]-*N*-[5-(8-Hydroxyquinoline)-acetyl]amino}acetate (Fmoc-aeg(hq)-O*t*Bu) (3).** In an ice bath and under N_2, 5-(8-Hydroxyquinolyl)acetic acid hydrochloride (6.6 g, 28 mmol), EDC (5.3 g, 28 mmol), HOBT (3.7 g, 28 mmol) were added to 200 mL of dry dichloromethane. After stirring for 15 min, DIPEA (9.6 mL, 55 mmol) was added, and the yellow solution was stirred for another 45 min. Fmoc-aeg-O*t*Bu·HCl (5.9 g, 14 mmol) was added, and the solution was stirred for 48 h at room temperature. The reaction mixture was washed with water (3 × 50 mL). The organic layer was dried over sodium sulfate, and the solvent was removed under vacuum. The crude product was purified using silica column chromatography with a 5% methanol in dichloromethane mobile phase; like fractions were combined, and the solvent was evaporated to yield a white foam (4.8 g, 64%). (ESI+) MS calculated: $[M+H]^+$ = 582.3; found $[M+H]^+$ = 582.2. ^{1}H NMR (400 MHz, $CDCl_3$): δ = 1.40 (m, 9H), 2.16 (s, 1H), 3.25−4.43 (m, 11H), 7.02−8.86 (m, 13H) ppm.

***Tert*-butyl{*N*-[2-Aminoethyl]-*N*-[5-(8-Hydroxyquinoline)-acetyl]amino}acetate (NH_2-aeg(hq)-O*t*Bu) (4).** This synthesis was adapted from a published procedure.[17] To Fmoc-aeg(hq)-O*t*Bu (4.8 g, 8.8 mmol), 480 mL of 20% piperidine in acetonitrile was added dropwise. The solution was stirred for 1 h and extracted with hexanes (3 × 100 mL). The acetonitrile layer was reduced by vacuum to yield a yellow oil. The crude

dx.doi.org/10.1021/ic3004504 | *Inorg. Chem.* 2012, 51, 11315−11323

product was purified using silica column chromatography with a 10% methanol in dichloromethane mobile phase; like fractions were combined, and the solvent was evaporated to yield a yellow oil (1.8 g, 57%). (ESI+) calculated: $[M+H]^+$ = 360.2; found $[M+H]^+$ = 360.3. ^{1}H NMR (300 MHz, $CDCl_3$): δ = 1.37 (m, 9H), 2.60 (m, 2H), 3.11 (s, 2H), 3.35 (m, 2H), 3.78 (s, 2H), 7.10 (d, J = 8 Hz, 1H), 7.36 (d,J = 8 Hz, 1H), 7.46 (q, J_1= 4 Hz, J_2 = 8 Hz, 1H), 8.30 (d, J = 8 Hz, 1H), 8.75 (d,J = 4 Hz, 1H) ppm.

***Tert*-butyl-aeg(hq)(hq)aeg(hq)-*tert*-butyl (5).** In an ice bath under nitrogen, **2** (0.74 g, 2.3 mmol), EDC (1.33 g, 7.0 mmol), HOBT (0.94 g, 7.0 mmol) were added to 100 mL of dry dichloromethane. The suspension was stirred for 15 min, DIPEA (2.42 mL, 13.9 mmol) was added, and the yellow solution was stirred for another 45 min. Compound **4** (2.5 g, 7.0 mmol) in 50 mL of dry dichloromethane was added, and the solution was allowed to stir for 4 d at room temperature. The solvent was removed under vacuum. The crude product was purified using silica column chromatography with a gradient mobile phase of 0% to 40% methanol in dichloromethane; like fractions were combined, and the solvent was evaporated to yield yellow foam (620 mg, 27%). (ESI+) MS calculated: $[M+H]^+$ = 1001.4; found $[M+H]^+$ = 1001.7.^{1}H NMR (400 MHz, $CDCl_3$): δ = 1.42 (m, 18H), 2.66 (m, 4H), 3.17 (s, 4H), 3.27 (m, 4H), 3.39 (s, 2H), 3.86 (s, 4H), 4.10 (m, 4H), 6.97 (m, 3H), 7.28 (m, 3H), 7.38 (m, 3H), 8.29 (m, 3H), 8.67 (m, 3H) ppm. 2D NMR data are listed in Supporting Information, Table S1 and Figures S2−S4. Elemental Anal. [**5**·2H_2O] Calcd: 61.38 C; 6.22 H; 10.80 N. Found: 61.50 C; 6.62 H; 11.00 N.

Zinc-Tripeptide Complex (Zn_3(5)$_2$). Zinc acetate (10.5 mg, 0.058 mmol) was dissolved in 2 mL of methanol. Hq-Tripeptide **5** (38.5 mg, 0.039 mmol) in 1 mL of methanol was added, and the resulting solution was stirred overnight. The solution was concentrated to a volume of 1.5, and 2 mL of water was added. A yellow precipitate began to form and was collected by centrifugation and decantation of the supernatant, washed with diethyl ether, and dried under vacuum. The product appeared to be a yellow solid (35.6 mg, 85%). (ESI+) MS calculated: $[Zn_3(C_{102}H_{106}N_{16}O_{24}) + 2H]^{2+}$ = 1069.7842 ; found $[Zn_3(C_{102}H_{106}N_{16}O_{24}) + 2H]^{2+}$ = 1069.7690. ^{1}H NMR (300 MHz, $CDCl_3$): δ = 1.05−1.50 (m, 36H), 2.00−4.65 (m, 44H), 6.00−9.65 (br, 30H) ppm. Elemental Anal. [**Zn_3(5)$_2$**· 6 H_2O] Calcd: 55.34 C; 5.52 H; 9.74 N. Found: 54.57 C; 5.81 H; 9.28 N.

Zinc-Monomer Complex (Zn(1)$_2$). Zinc acetate (18.3 mg, 0.10 mmol) was dissolved in 2 mL of methanol. Monomer **1** (50.0 mg, 0.13 mmol) in 1 mL of methanol was added, and the resulting solution was stirred overnight. The solution was concentrated to a volume of 1.5, and 2 mL of water was added. A yellow precipitate began to form and was collected by centrifugation and decantation of the supernatant, washed with diethyl ether, and dried under vacuum. The product appeared to be a yellow solid (44.2 mg, 84%). (ESI+) MS calculated: $[Zn(C_{38}H_{42}N_4O_{12}) + H]^+$ = 810.2073; found $[Zn(C_{38}H_{42}N_4O_{12}) + H]^+$ = 810.1937.^{1}H NMR (400 MHz, CD_3OD): δ = 1.15 (br, 12H), 3.59 (s, 4H), 3.75−4.10 (m, 16H), 6.62−7.74 (m, 6H), 8.10−8.97 (m, 4H) ppm. Elemental Anal. [**Zn(2)$_2$**·2H_2O] Calcd: 53.81 C; 5.47 H; 6.61 N. Found: 54.57 C; 5.02 H; 7.18 N.

Methods. UV−visible absorbance spectra were obtained with a double-beam spectrophotometer (Varian, Cary 500). Emission spectra were measured using a Photon Technology International (PTI) fluorescence spectrometer using an 814 photomultiplier detection system. Quantum yields were determined using the relationship:[18]

$$\Phi = \Phi_{ref}\frac{(I/A)}{(I_{ref}/A_{ref})}\left(\frac{\eta}{\eta_{ref}}\right)^2 \quad (1)$$

where Φ is the radiative quantum yield of the sample, Φ_{ref} is the known quantum yield of anthracene in ethanol, 0.27, I is the integrated emission, A is the absorbance at the excitation wavelength, and η is the refractive index of the solvent, which is assumed to be the same for the methanol solutions of sample and reference.

Time resolved emission decays were measured following excitation using a N_2 dye laser (PTI model GL-302), averaging 5 decays with a 50 μs collection time per point. Steady-state fluorescence anisotropy experiments were performed using the PTI fluorescence spectrometer equipped with motorized polarizers. Anisotropy (r) and polarization (P) are defined by[19]

$$r = \frac{I_{VV} - GI_{VH}}{I_{VV} + 2GI_{VH}}; \quad P = \frac{3r}{2 + r} \quad (2)$$

where I_{VV} is the light intensity with excitation and emission polarizer vertically aligned; I_{VH} uses an excitation polarizer vertical and the emission polarizer horizontal. G is the intensity ratio of the vertical to horizontal components of the emission when the sample is excited with horizontally polarized light (G =I_{HV} /I_{HH}).

Spectrophotometric absorbance and emission titrations were conducted in spectroscopic grade methanol solutions at room temperature, in the presence of air, using known concentrations of peptide compounds. In the emission spectra, the compounds were excited at their $\pi-\pi^*$ transition absorbance maxima (λ_{ex} = ~326 nm) and monitored at their emission maxima (λ_{em} = ~423 nm). The Zn complexes were excited at the $\pi-\pi^*$ absorbance maxima (λ_{ex} = ~391 nm) and monitored at their emission maxima (λ_{em} = ~567 nm). During the spectrophotometric titration, absorbance and emission spectra were obtained after stirring the solution with each known volume (3.3−10 μL) of standard 15 mM $Zn(OAc)_2$ solutions in methanol for 10 min.

NMR spectra were collected using either a 300 or a 400 MHz spectrometer (Bruker) in the Lloyd Jackman Nuclear Magnetic Resonance Facility. Elemental analyses were performed by Galbraith Industries. Mass spectrometric analyses were performed on a Waters LCT Premier time-of-flight (TOF) mass spectrometer at the Penn State Mass Spectrometry Facility. Samples were introduced into the mass spectrometer using direct infusion via a syringe pump, and the spectrometer was scanned from 200 to 2500 m/z in positive ion mode using electrospray ionization (ESI+).

A molecular model was generated using a full geometry optimization performed in vacuum using HyperChem (Version 6, HyperCube Inc.) with the MM+ force field. The steepest descent algorithm and a termination condition with a rms gradient of 0.1 kcal mol^{-1} Å^{-1} were employed during the optimization.

RESULTS AND DISCUSSION

Synthesis of Hq-Tripeptide. Our group has previously synthesized different sequences of oligopeptides via solid[7a,b,8a] and solution[7c,8b−d,9] phase techniques, which sequentially

Scheme 2. Synthetic Steps toward hq-tripeptide 5[a]

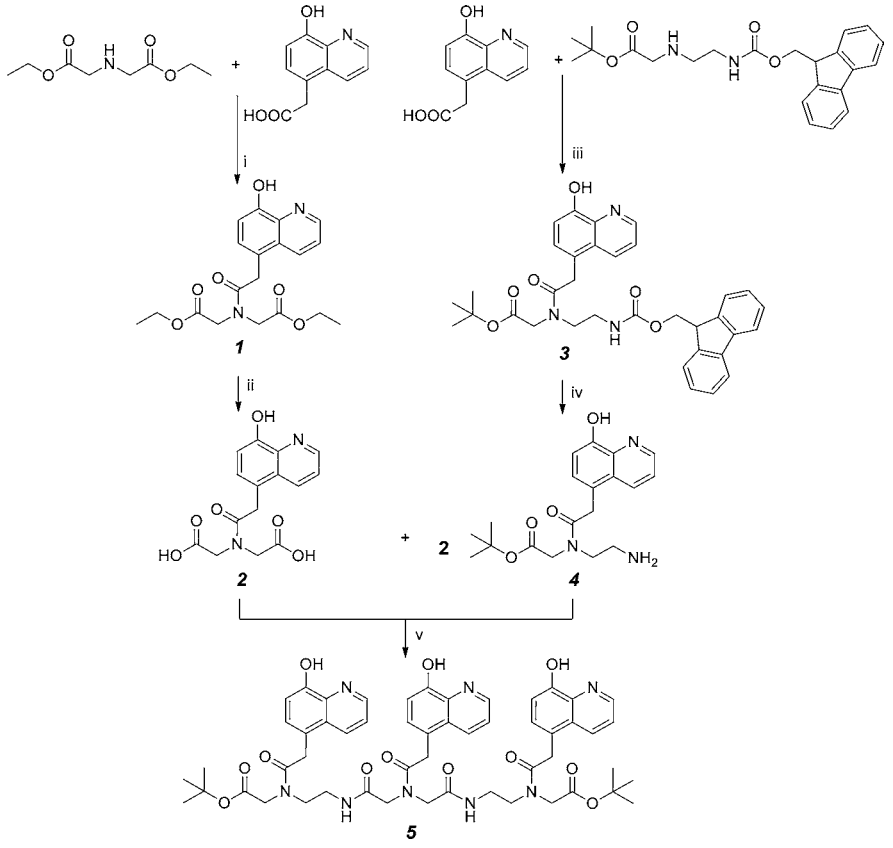

[a](i) EDC, HOBT, DIPEA, CH_2Cl_2, 2 d, rt; (ii) 2M NaOH, THF, overnight, rt; (iii) EDC, HOBT, DIPEA, CH_2Cl_2, 2 d, rt; (iv) 20% piperidine in acetonitrile, 1 h, rt; (v) EDC, HOBT, DIPEA, CH_2Cl_2, 4 d, rt.

install monomer units on one terminus of the chain. The modified approach taken in this work utilizes a more efficient synthetic route that allows for a one-pot synthesis of a tripeptide from a diacid terminated monomer building block.[8e] Scheme 2 contains the synthetic steps to synthesize the tripeptide. The synthesis of the central monomer begins with an ethyl ester protected iminodiacetic acid backbone and couples to it a pendant acetic acid containing a hydroxyquinoline ligand to afford a central monomer **1**. Acid deprotection of **1**, and subsequent reaction with amine-terminated hydroxyquinoline monomer **4**, gives hq-tripeptide **5** in a 27% yield. High-resolution electrospray ionization mass spectrometry was used to identify the product by evaluation of the molecular ion peak with respect to the theoretical mass/charge ratio for the tripeptide ($[M+H]^+$ m/z: calculated 1001.4, found 1001.4). In the ^{1}H NMR spectrum of tripeptide **5**, the observed proton integrations (15 aromatic, 22 aliphatic, 18 *tert*-butyl protons) are consistent with the tripeptide structure shown in Scheme 2. Detailed analysis of the ^{1}H-^{1}H COSY spectrum of **5** (Supporting Information, Figure S2–2) shows correlations between neighboring protons on aromatic rings that enables assignment of the proton peaks together with comparisons between the ^{1}H NMR spectra of **5**, and monomers **2** and **4** (Supporting Information, Figure S1–2). The elemental analysis of **5** reveals the presence of water, consistent with all artificial oligopeptides we have reported,[7–9] and indicative of their hygroscopic behavior. These data, together with the ^{13}C–^{1}H HMBC (Supporting Information, Figure S3) and ^{13}C-^{1}H HMQC (Supporting Information, Figure S4), confirm the identity and purity of the tripeptide structure.

Synthesis of Zinc Hq-Tripeptide Complex. To investigate oligopeptide-directed assembly of a multimetallic structure, tripeptide **5** was reacted with zinc acetate. The resulting yellow powder was precipitated in methanol/water solution, washed copiously with diethyl ether, and dried under vacuum at room temperature. For comparison, the Zn complex of monomer **1** was synthesized under identical reaction conditions. The Zn complexes of **1** and **5** were characterized by ^{1}H NMR spectroscopy, mass spectrometry, and elemental analysis. In both cases, the molecular ion peak observed by ESI + mass spectrometry is consistent with formation of the $[Zn(\mathbf{1})_2]$ and $[Zn_3(\mathbf{5})_2]$ complexes (Supporting Information, Figure S5). However, in the ESI+ MS of the trimetallic structure, the mass of the molecular ion indicated cleavage of one of the four *t*-butyl chain termini, and the fully intact $[Zn_3(\mathbf{5})_2]$ molecular ion was not observed. This is most likely a result of difficulty in volatilizing the large, charge-neutral complex together with gas phase instability of the ionized structure, rather than cleavage of the *t*-butyl esters in solution. Evidence to support this is gained from the ^{1}H NMR spectra of the Zn complexes. In these, the presence of bound Zn results in broadening of the proton peaks, particularly in the aromatic region. Integration of the peaks and comparison of aliphatic and aromatic regions are however consistent with intact chains and the unmetalated oligopeptides.

It has been reported that Zn complexes of unsubstituted 8-hydroxyquinolines form octahedral structures with two axial

dx.doi.org/10.1021/ic3004504 | *Inorg. Chem.* 2012, 51, 11315–11323

water molecules binding the square planar bis(quinolinato)zinc moiety.[20] Conversely, crystal structures of *anhydrous* 8-quinolinate complex of zinc(II) reveal $[Zn(hq)_2]$ units connected by bridging quinolinate oxygen atoms.[21] Our synthetic conditions are not water free: after extended drying under vacuum the ^{1}H NMR spectrum contains a proton peak assigned to water. The elemental analysis of the $[Zn_3(\mathbf{5})_2]$ and $[Zn(\mathbf{1})_2]$ complexes reveals the presence of excess H and O atoms: in comparison with the expected analysis for anhydrous $[Zn_3(\mathbf{5})_2]$, the C and N are ~3% and 1% lower, and H is 0.6% higher. This may be a result of water molecules that are bound in the structure, either in the axial positions or hydrogen bonded with the backbone. That these are not observed in the mass spectrum suggests that they are easily dissociated in the gas phase.

Because we have been unable to form high quality crystals, to visualize and understand the structure, the molecular model in Figure 1 was calculated using HyperChem. This model suggests

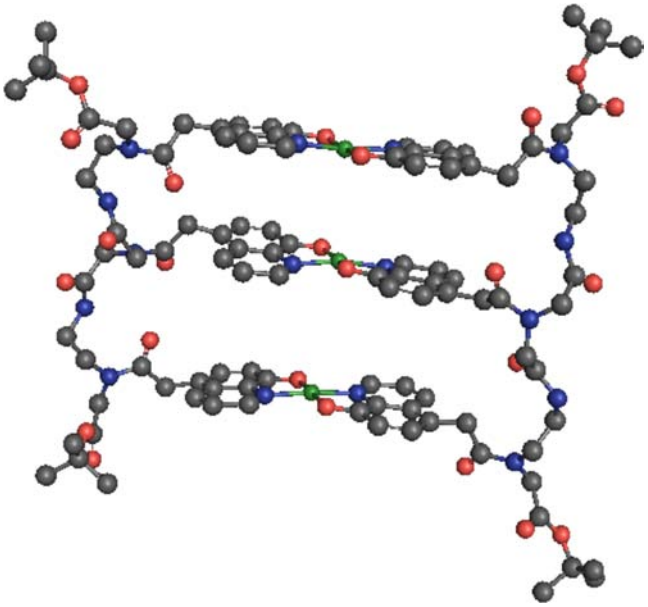

Figure 1. Molecular model calculated with a MM+ force field $Zn_3(5)_2$, with the Zn(II) centers shown in green.

that the low energy conformation holds the Zn complexes ~6 Å apart. Despite π-interactions between hq ligands on adjacent complexes that would be favorable for inducing order and crystallization, the free rotation around the acetyl bonds that link each hq ligand to the backbone allows the formation of geometric isomers. Figure 1 shows only one geometric isomer, and is realistic in that it reveals a variable relative orientation of the acetyl groups.

Figure 1 does not show solvent molecules; however, it shows that access to the inner Zn complex is sterically hindered by the flanking Zn complexes and tripeptides, and that as a result it is unlikely that each of the three Zn complexes has two axial water or solvent molecules. The model suggests that it is feasible that the solvation of the inner Zn complex differs from the outer Zn complexes, and that isomers exist with varied locations of axial water molecules. To attempt to eliminate the ambiguity about the location of water molecules within the structure, separate reactions were conducted that were strictly anhydrous or heated to high temperatures. However the products of the reaction of Zn and (mono- or tri-) peptide under these conditions were found to be amorphous powders that were completely insoluble and were not further characterized. Because the room temperature methanolic solutions formed soluble Zn complexes that could be characterized and studied using spectroscopic methods, and because the elemental analysis, mass spectrometry, and NMR data taken together confirm formation of the $[Zn_3(\mathbf{5})_2]$ and $[Zn(\mathbf{1})_2]$ complexes with included water, these were used in all further investigations.

Photophysical Behavior. Hydroxyquinoline was selected for insertion into our structures because of its well-known photophysical behavior. Zinc hydroxyquinoline metal chelates are electroluminescent and are used in organic light emitting diodes because of their high thermal stability, bright fluorescence, and excellent electron-transport mobility in the solid state.[11e] To begin to investigate the properties of the peptide-linked structures, absorption and emission spectra were obtained, and the data for **1**, **5**, $[Zn(\mathbf{1})_2]$, and $[Zn_3(\mathbf{5})_2]$ are summarized in Table 1. Compounds **1** and **5** have similar

Table 1. Photophysical Data for 1, 5, $[Zn(\mathbf{1})_2]$, and $[Zn_3(\mathbf{5})_2]$

	1	**5**	$[Zn(\mathbf{1})_2]$	$[Zn_3(\mathbf{5})_2]$
$\lambda_{max,\ abs}$ (nm)[a]	325	326	390	391
ε, M^{-1} cm^{-1} × 10^3	3.07	7.18	5.86	14.1
$\lambda_{max,\ em}$ (nm)[b]	423	423	565	567
Φ[c]	0.0014	0.0053	0.031	0.14
τ (ns)[d]	1.3 ± 0.5	1.4 ± 0.5	3.8 ± 0.2	4.6 ± 0.2
r[e]			0.029	0.042
P[f]			0.043	0.062

[a]Maximum absorbance wavelength and extinction coefficient for the $\pi-\pi^*$ transition band in methanol. [b]Peak emission wavelength following excitation at $\lambda_{max,\ abs}$ in methanol. [c]Emission quantum yields following excitation at $\lambda_{max,\ abs}$ in methanol, determined using anthracene in ethanol (Φ = 0.27) as a reference. [d]Emission lifetime determined from a single exponential fit to the time-resolved decay at the maximum emission wavelength in methanol. [e,f]Fluorescence anisotropy (r) and polarization (P) determined at $\lambda_{max,\ em}$ following excitation at $\lambda_{max,\ abs}$ in methanol.

absorbance spectra, with peaks at 326 nm that are assigned to the $\pi-\pi^*$ transition of the 8-hydroxyquinoline ligand.[22] Excitation of the compounds at their absorbance maxima gives rise to emission with a peak wavelength of 423 nm. The absorption and emission maxima suggest that under these conditions there is no formation of excitons in the tripeptide, because of the absence of a red-shifted emission.

Complexation of Zn(II) to form $[Zn(\mathbf{1})_2]$ and $[Zn_3(\mathbf{5})_2]$ changes the electronic distribution in the ligands and results in red shifts of both the absorption and the emission maxima to 391 nm and ~567 nm, respectively, for both compounds. The comparable absorbance and emission spectra for the $[Zn(\mathbf{1})_2]$ and $[Zn_3(\mathbf{5})_2]$ complexes imply that they are in the same electronic environments. However, the absorbance spectrum of the $[Zn_3(\mathbf{5})_2]$ structure contains new peaks in the 290 nm −310 nm region that are not present in the spectrum of $[Zn(\mathbf{1})_2]$; similarly tripeptide **5** has an absorbance peak at 284 nm that monomer **1** does not have. The presence of the high-energy peak in the multifunctional structure is suggestive of interactions between pendant hq ligands on the backbone, perhaps by the π stacking of neighboring pyridyl rings.[23]

When solutions of known concentration are used, the extinction coefficients (ε) of **5** and $[Zn_3(\mathbf{5})_2]$ are found to be

dx.doi.org/10.1021/ic3004504 | *Inorg. Chem.* 2012, 51, 11315−11323

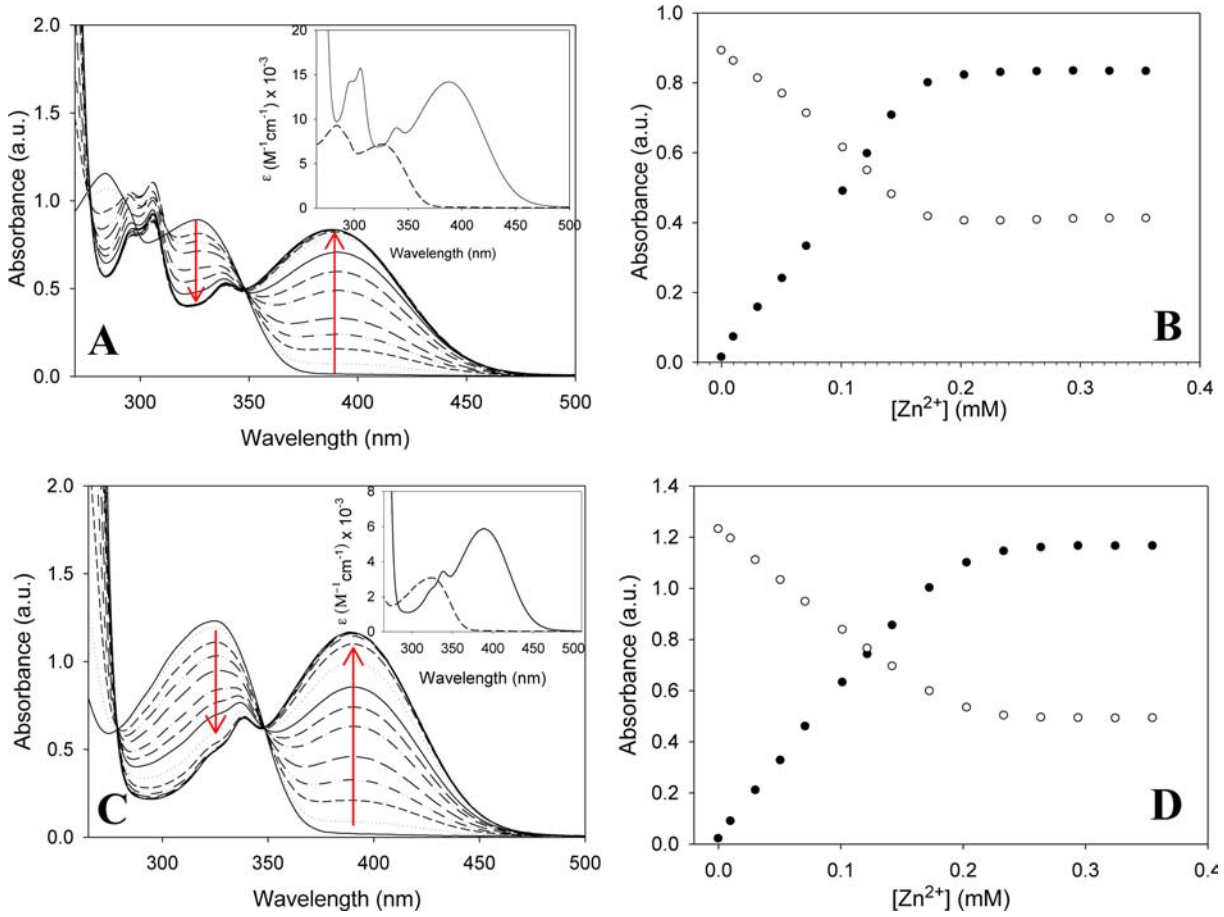

Figure 2. (A) UV−vis absorbance spectra for the titration of 5.0 mL of 0.13 mM tripeptide **5** with 3.3−10 μL injections of 15 mM $Zn(OAc)_2$ in methanol. Inset: Extinction spectra of the tripeptide **5** (dashed line) and $[Zn_3(\mathbf{5})_2]$ (solid line) in methanol solutions. (B) Titration curves during this titration, monitored at 326 nm (○) and 391 nm (●). (C) UV−vis absorbance spectra for the titration of 5.0 mL of 0.35 mM monomer **1** with 3.3−10 μL injections of 15 mM $Zn(OAc)_2$ in methanol. Inset: Extinction spectra of the monomer **1** (dashed line) and Zn monomer complex $[Zn(\mathbf{1})_2]$ (solid line) in methanol solutions. (D) Titration curves for the addition of Zn(II) into 5.0 mL of 0.35 mM monomer **1**, monitored at 325 nm (○) and 390 nm (●).

2.5 times higher than those measured for **1** and $[Zn(\mathbf{1})_2]$, respectively (Supporting Information, Figure S7). Although lower than the expected ratio of 3 based on the oligomer length, the slightly depressed extinction may be a result of a hypochromic effect, as commonly seen in DNA, RNA, and polymers.[24] The emission quantum yields (Φ) of **5** and $[Zn_3(\mathbf{5})_2]$ are about 4 times larger than those for **1** and $[Zn(\mathbf{1})_2]$, respectively. However, the excited state lifetimes of the monomer and tripeptide are short and equivalent within the experimental error and resolution of the instrument. Complexation of Zn increases the excited state lifetime of the hq excited state, and the measured lifetimes for the $[Zn(\mathbf{1})_2]$ and $[Zn_3(\mathbf{5})_2]$ complexes are approximately the same. The greater quantum yield of the $[Zn_3(\mathbf{5})_2]$ complex may be a result of shielding of the central fluorophore from solvent, caused by the close proximity of the aromatic and charge neutral complexes within the assembly. Similar fluorescence enhancement has been observed in folded oligopeptides that create a hydrophobic local environment for inserted fluorophores.[25]

Polarization anisotropy was further used to probe the differences in chromophore size, since lower anisotropy or polarization values are indicative of faster molecular rotation. As indicated in Table 1, the $[Zn(\mathbf{1})_2]$ complex has a lower anisotropy value compared to $[Zn_3(\mathbf{5})_2]$ (0.029 vs 0.042, respectively). Both values compare well with the measured anisotropy value of a 13 bp duplex DNA duplex (~ 0.04).[26] These data are consistent with the formation of a larger structure when the tripeptide binds zinc, creating a molecule with slower rotational diffusion.

Determination of Stoichiometry. Because hydroxyquinoline is capable of a variety of coordination geometries, it is important to separately determine the stoichiometry of Zn to ligand for the duplex. Figures 2A and C contain the absorption spectra upon iterative addition of metal ions to solutions of **5** and **1**, respectively. In each case, addition of Zn(II) results in a strong red-shift in the peak absorbance wavelength from 326 to 391 nm; these maxima are identical to those separately measured for the pure compounds (Table 1). The spectrophotometric titrations further reveal a clear isosbestic point at 350 nm, indicative of the clean conversion of one species to another.

The highly emissive nature of the hq ligand and $[Zn(hq)_2]$ complexes also enables the monitoring of the reaction stoichiometry by emission titrations. Figure 3A shows that for compound **5**, emission is initially bright but incremental addition of Zn(II) to the solution causes the emission intensity at 423 nm to decrease, while a new emission peak at 561 nm concurrently forms and increases in intensity. When the solution is excited at 391 nm, the emission maximum red-shifts to 567 nm and the intensity of the peak increases (Figure

dx.doi.org/10.1021/ic3004504 | *Inorg. Chem.* 2012, 51, 11315−11323

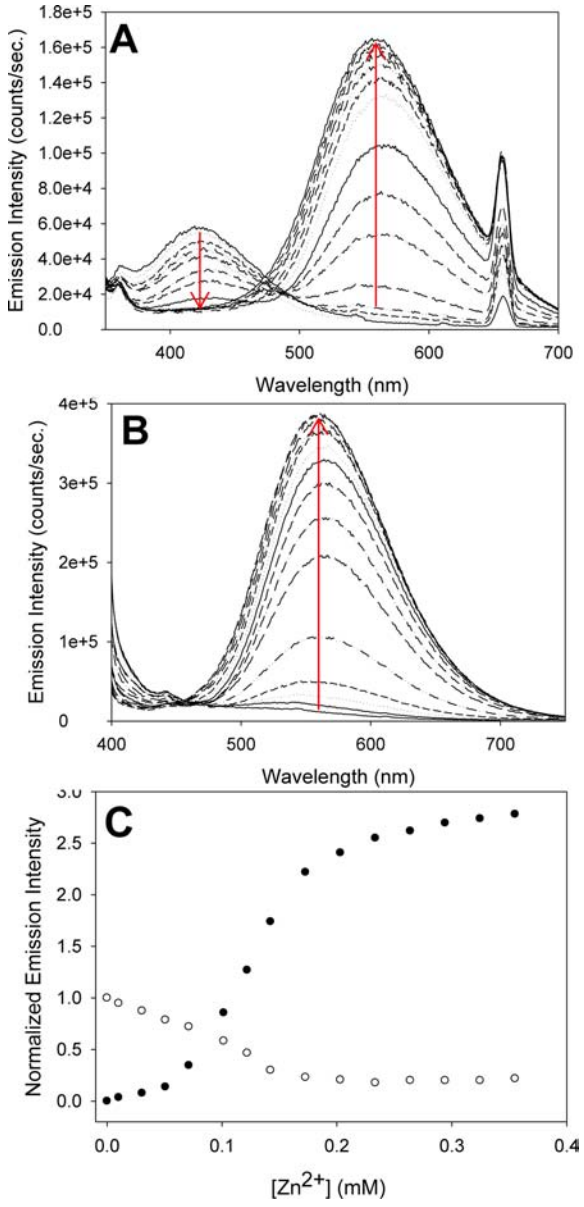

Figure 3. (A) Fluorescence emission spectra during the titration of 5.0 mL of 0.13 mM tripeptide **5** with 3.3−10 μL injections of 15 mM $Zn(OAc)_2$ in methanol using an excitation wavelength of 326 nm. (B) Fluorescence emission spectra for the titration of 5.0 mL of 0.13 mM tripeptide **5** with 3.3−10 μL injections of 15 mM $Zn(OAc)_2$ in methanol at an excitation wavelength of 391 nm. (C) Titration curves for the addition of Zn(II) into 5.0 mL of 0.13 mM tripeptide **5**, monitored at 423 nm (○) and 561 nm (●).

3B), whereas emission at 423 nm is no longer observed. Analogous experiments using monomer **1** have identical spectral features, and are shown in the Supporting Information. The excitation and emission maxima measured for pure **5** and $[Zn_3(\mathbf{5})_2]$ are identical to those observed during the titration in Figure 3.

Figures 2B and D contain the titration plots while monitoring the absorption of the ligand at 325 nm and the Zn complex at 390 nm, as a function of the concentration of added Zn^{2+}. Both plots exhibit a linear trend as metal ion is added until the equivalence point is reached, at which point the absorption remains constant. In Figures 2B and D, the equivalence points occur at Zn(II) concentrations of ~0.19 mM with 0.13 mM tripeptide **5**, and ~0.2 mM Zn(II) with 0.35 mM monomer **1**. Figure 3C contains the separately measured titration plot monitoring the *emission* intensity at λ_{em} = 423 and 561 nm during addition of Zn(II) to **5**. Like the absorption titration curves, the addition of Zn into 0.13 mM tripeptide **5** induces changes in the emission intensity that level at a concentration of ~0.19 mM Zn(II). Taken together, the separately measured absorption and emission titration data reveal a reaction stoichiometry of $Zn(II)^{2+}$ with tripeptide **5** of 3 Zn: 2 tripeptide, whereas the analogous experiment with monomer **1** gives a molar ratio of 1 Zn: 2 monomer (see Supporting Information for emission titration).

Using the absorbance at 390 nm and concentration of Zn(II) at the equivalence point in Figure 2B and D, the extinction coefficients of the formed species are ~4600 for **5** and 5600 M^{-1} cm^{-1} for **1**. The latter of these compares favorably with the measured extinction coefficient of pure $[Zn(\mathbf{1})_2]$ (Table 1), confirming that the species formed during this titration is the $[Zn(\mathbf{1})_2]$ complex. During the titration of tripeptide **5**, the extinction coefficient at the equivalence point is written in terms of the total concentration of Zn(II). Because pure $[Zn_3(\mathbf{5})_2]$ contains 3 Zn/molecule, the measured value of ε must be normalized to the total concentration of zinc for comparison of the titration product (Figure 2B), giving 14100/3 = 4700 M^{-1} cm^{-1} for pure $[Zn_3(\mathbf{5})_2]$. As a result, the extinction coefficient of the product of the titration in Figure 2B is in fact in excellent agreement with that of pure $[Zn_3(\mathbf{5})_2]$. Together with the clean isosbestic point and reaction stoichiometry, these data are consistent with the formation of three Zn bis(hydroxyquinoline) complexes linking strictly two tripeptide strands to give $[Zn_3(\mathbf{5})_2]$ during the titration.

Equilibrium Constants and Cooperativity. In oligomers and polymers, it is well-known that multisite binding can lead to changes to the binding equilibria as result of positive or negative cooperativity.[25,26] The distinct peaks in both the absorption and the emission spectra for the hq ligand and its Zn complexes enable the quantitative measurement of the association equilibrium constant, K_a, which is given by

$$K_a = \frac{[Zn(Hq)_2]}{[Zn^{2+}][Hq]^2} \quad (3)$$

Figure 4A contains working plots with slopes equal to the equilibrium constants, using concentrations of the species that are determined from the emission titrations. The slopes of the two curves at low concentration are approximately the same. However, whereas the curve for monomer **1** is linear, addition of Zn(II) to tripeptide **5** gives a curve that becomes nonlinear at high concentrations of zinc. The steeper slope at increasing Zn(II) concentrations suggests a greater affinity, and is typically analyzed by use of the Hill equation:[27]

$$\log \frac{\theta}{1-\theta} = n \log[Zn^{2+}] - \log K_d \quad (4)$$

where K_d is the apparent dissociation constant, n is the Hill coefficient, and

$$\theta = 2\frac{[Zn(hq)_2]}{[Hq]^0} \quad (5)$$

Figure 4B contains the Hill plots of tripeptide **5** and monomer **1** over a concentration range of 15%−85%. While the slope of the monomer **1** Hill plot is n = 1.3, the Hill plot for **5** has a marked sigmoidal shape with a slope of n = 3.5 around

dx.doi.org/10.1021/ic3004504 | *Inorg. Chem.* 2012, 51, 11315−11323

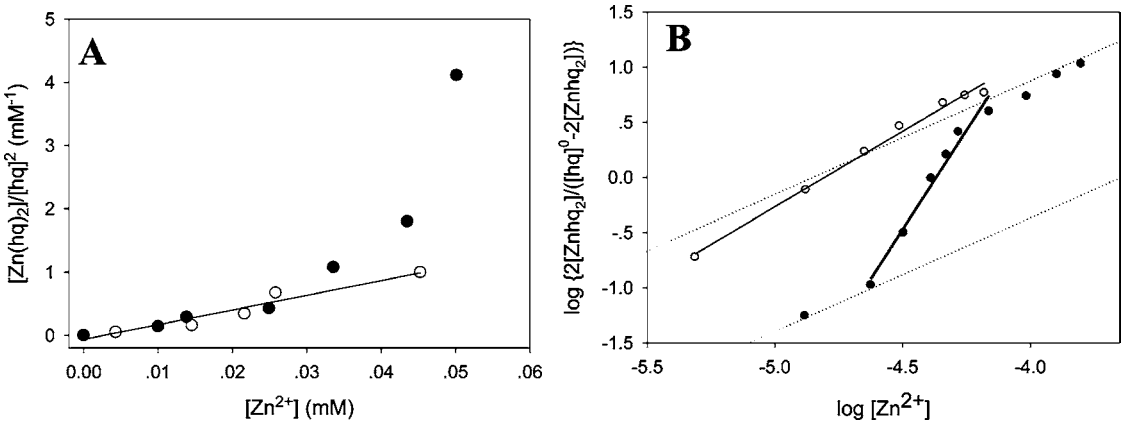

Figure 4. (A) Emission working plots of the tripeptide **5** (●) and monomer **1** (○), from which the equilibrium constants are determined. The solid line is the linear fitting curve of the monomer. (B) Hill plots of the tripeptide **5** (●) and the monomer **1** (○). The data are fitted (solid lines) over the range of 15% to 85% saturation. Dotted lines indicate a reference trend with slope = 1.

50% saturation. These values are identical to those obtained from Hill plots constructed from the absorbance titration experiments (see Supporting Information). The higher value of n for **5** is indicative of positive cooperativity during coordination of Zn.[28] When the intercepts of the plots in Figure 4B are used, the association coefficients (i.e., $K_a = (1/K_d)^{2/n}$) are determined to be $K_a = 1.0 \times 10^9$ and $K_a = 1.6 \times 10^8$ (L^2 mol^{-2}) for Zn binding by tripeptide **5** and monomer **1**, respectively. These values compare favorably to the values measured for both the bis(8-quinolinolato) zinc(II) and the multihydroxyquinoline-armed complexes.[29] The analogous data from the absorbance titrations (see Supporting Information) give values of $K_a = 2.1 \times 10^9$ and $K_a = 9.7 \times 10^7$ L^2 mol^{-2} for **5** and **1**, respectively, and are in excellent agreement with the emission data. These studies quantitatively confirm that cooperative formation of multiple $[Zn(hq)_2]$ bridges between the oligopeptide strands results in a structure with greater stability than the monometallic analogue.

Cooperative formation of the highly stable $[Zn_3(\mathbf{5})_2]$ complex to give a structure with fluorescence emission and higher quantum yields compared to its monometallic analogue suggests that extended structures containing many $[Zn(hq)_2]$ would be both straightforward to assemble and give bright emitters. Such structures have potential uses in materials that require multiple chromophores such as sensors and energy transfer antennas. The tunable aeg structure is amenable to preparing longer oligopeptides with varying ligand sequences. Our continuing efforts seek to determine the role of structure on the stability and photodynamics of multichromophore structures. This detailed study provides fundamental understanding about metal coordination-based molecular recognition for the future design of photonic wires and light-harvesting antennas in multimetallic and multichromophore structures that could ultimately be useful in sensors, artificial photosynthesis, and for conversion of solar energy.

■ ASSOCIATED CONTENT

Ⓢ Supporting Information

^{1}H and 2-D NMR spectra, NMR peak assignments, and additional visible absorption and emission spectra. This material is available free of charge via the Internet at http://pubs.acs.org.

■ AUTHOR INFORMATION

Corresponding Author

*E-mail: mbw@chem.psu.edu.

Notes

The authors declare no competing financial interest.

■ ACKNOWLEDGMENTS

We gratefully acknowledge financial support from Chemical Sciences, Geosciences and Biosciences Division of the Office of Basic Energy Sciences of the U.S. Department of Energy (DE-FG02-08ER15986).

■ REFERENCES

(1) (a) Schlicke, B.; Belser, P.; Cola, L. D.; Sabbioni, E.; Balzani, V. *J. Am. Chem. Soc.* **1999**, *121*, 4207−4214. (b) Yan, H.; Park, S. H.; Finkelestein, G.; Reif, J. H.; LaBean, T. H. *Science* **2003**, *301*, 1882−1884. (c) Malvankar, N. S.; Vargas, M.; Nevin, K. P.; Franks, A. E.; Leang, C.; Kim, B. C.; Inoue, K.; Mester, T.; Covalla, S. F.; Johnson, J. P.; Rotello, V. M.; Tuominen, M. T.; Lovley, D. R. *Nat. Nanotechnol.* **2011**, *6*, 573−579.

(2) (a) Steinberg-Yfrach, G.; Rigaud, J. L.; Durantini, E. N.; Moore, A. L.; Gust, D.; Moore, T. A. *Nature* **1998**, *392*, 479−482. (b) Bennett, I. M.; Farfano, H. M.; Bogani, F.; Primak, A.; Liddell, P. A.; Otero, L.; Sereno, L.; Silber, J. J.; Moore, A. L.; Moore, T. A.; Gust, D. *Nature* **2002**, *420*, 398−401. (c) Kuciauskas, D.; Liddell, P. A.; Lin, S.; Johnson, T. E.; Weghorn, S. J.; Lindsey, J. S.; Moore, A. L.; Moore, T. A.; Gust, D. *J. Am. Chem. Soc.* **1999**, *121*, 8604−8614.

(3) Balzani, V. *Electron Transfer in Chemistry*; Wiley: Weinheim, Germany, 2001; Vol. *5*, pp 97−136.

(4) (a) Wasielewski, M. R. *J. Org. Chem.* **2006**, *71*, 5051−5066. (b) Li, X.; Sinks, L. E.; Rybtchinski, B.; Wasielewski, M. R. *J. Am. Chem. Soc.* **2004**, *126*, 10810−10811.

(5) Huynh, M. H. V.; Dattelbaum, D. M.; Meyer, T. J. *Coord. Chem. Rev.* **2005**, *249*, 457−483.

(6) Nielsen, P. E.; Haaima, G. *Chem. Soc. Rev.* **2007**, *26*, 73−78.

(7) (a) Gilmartin, B. P.; Ohr, K.; McLaughlin, R. L.; Koerner, R.; Williams, M. E. *J. Am. Chem. Soc.* **2005**, *127*, 9546−9555. (b) Ohr, K.; Gilmartin, B. P.; Williams, M. B. *Inorg. Chem.* **2005**, *44*, 7876−7885. (c) Levine, L. A.; Youm, H. W.; Yennawar, H. P.; Williams, M. E. *Eur. J. Inorg. Chem.* **2008**, 4083−4091.

(8) (a) Ohr, K.; McLaughlin, R. L.; Williams, M. E. *Inorg. Chem.* **2007**, *46*, 965−974. (b) Gilmartin, B. P.; McLaughlin, R. L.; Williams, M. E. *Chem. Mater.* **2005**, *17*, 5446−5454. (c) Coppock, M. B.; Kapelewski, M. T.; Youm, H. W.; Levine, L. A.; Miller, J. R.; Myers, C. P.; Williams, M. E. *Inorg. Chem.* **2010**, *49*, 5126−5133. (d) Coppock, M. B.; Williams, M. E. *Inorg. Chem.* **2011**, *50*, 949−955. (e) Gallagher,

J. A.; Levine, L. A.; Williams, M. E. *Eur. J. Inorg. Chem.* **2011**, *27*, 4168−4174.
(9) (a) Levine, L. A.; Kirin, S. I.; Myers, C. P.; Showalter, S. A.; Williams, M. E. *Eur. J. Inorg. Chem.* **2009**, 613−621. (b) Myers, C. P.; Gilmartin, B. P.; Williams, M. E. *Inorg. Chem.* **2008**, *47*, 6738−6747. (c) Myers, C. P.; Miller, J. R.; Williams, M. E. *J. Am. Chem. Soc.* **2009**, *131*, 15291−15300.
(10) (a) Zeng, F.; Zimmerman, S. C. *Chem. Rev.* **1997**, *97*, 1681−1712. (b) Haba, Y.; Harada, A.; Takagishi, T.; Kono, K. *J. Am. Chem. Soc.* **2004**, *126*, 12760−12761. (c) Mattei, S.; Seiler, P.; Diederich, E.; Gramlich, V. *Heir. Chim. Acta* **1995**, *78*, 1904−1912. (d) Newkome, G. R.; Lin, X. *Macromolecules* **1991**, *24*, 1443−1444. (e) Crespo, L.; Sanclimens, G.; Pons, M.; Giralt, E.; Royo, M.; Albericio, F. *Chem. Rev.* **2005**, *105*, 1663−1681.
(11) (a) Brinkmann, M.; Gadret, G.; Muccini, M.; Taliani, C.; Masciocchi, N.; Sironi, A. *J. Am. Chem. Soc.* **2000**, *122*, 5147−5157. (b) Sapochak, L. S.; Padmaperuma, A.; Washton, N.; Endrino, F.; Schmett, G. T.; Marshall, J.; Fogarty, D.; Burrows, P. E.; Forrest, S. R. *J. Am. Chem. Soc.* **2001**, *123*, 6300−6307. (c) Thomsen, D. L.; Phely-Bobin, T.; Papadimitrakopoulos, F. *J. Am. Chem. Soc.* **1998**, *120*, 6177−6178. (d) Yin, S. G.; Hua, Y. L.; Chen, X. H.; Yang, X. H.; Hou, Y. B.; Xu, X. R. *Synth. Met.* **2000**, *111*, 109−112. (e) Du, N.; Tian, R.; Peng, J.; Lu, M. *J. Polym Sci: Part A* **2005**, *43*, 397−406.
(12) (a) Ma, Z.; Skorik, Y. A.; Achim, C. *Inorg. Chem.* **2011**, *50*, 6083−6092. (b) Watson, R. M.; Skorik, Y.; Patra, G. K.; Achim, C. *J. Am. Chem. Soc.* **2005**, *127*, 14628−14639.
(13) Pfeil, A.; Lehn, J. M. *J. Chem. Soc., Chem. Commun.* **1992**, 838−840.
(14) Warner, V. D.; Sane, J. N.; Mirth, D. B.; Turesky, S. S.; Soloway, B. *J. Med. Chem.* **1976**, *19*, 167−169.
(15) Thomson, S. A.; Josey, J. A.; Cadilla, R.; Gaul, M. D.; Hassman, C. F.; Luzzio, M. J.; Pipe, A. J.; Reed, K. L.; Ricca, D. J.; Wiethe, R. W.; Noble, S. A. *Tetrahedron.* **1995**, *51*, 6179−6194.
(16) Dueholm, K. L.; Egholm, M.; Behrens, C.; Christensen, L.; Hansen, H. F.; Vulpius, T.; Petersen, K. H.; Berg, R. H.; Nielsen, P. E.; Buchardt, O. *J. Org. Chem.* **1994**, *59*, 5767−5773.
(17) Nawrot, B.; Rebowska, B.; Cieslinska, K.; Stec, W. J. *Tetrahedron Lett.* **2005**, *46*, 6641−6644.
(18) Williams, A. T. R.; Winfield, S. A.; Miller, J. N. *Analyst* **1983**, *108*, 1067−1071.
(19) Valeur, B. *Molecular Fluorescence: Principles and Applications*; Wiley: New York, 2001; pp 125−167.
(20) (a) Merritt, L. L.; Cady, R. T.; Mundy, B. W. *Acta Crystallogr.* **1954**, *7*, 473−476. (b) Albrecht, M.; Witt, K.; Weis, P.; Wegelius, E.; Froehlich, R. *Inorg. Chim. Acta* **2002**, *341*, 25−32.
(21) Kai, Y.; Morita, M.; Yasuoka, N.; Kasai, N. *Bull. Chem. Soc. Jpn.* **1985**, *58*, 1631−1635.
(22) Moeller, T.; Cohen, A. J. *Anal. Chem.* **1950**, *22*, 686−690.
(23) (a) Brinkmann, M.; Gadret, G.; Muccini, M.; Taliani, C.; Masciocchi, N.; Sironi, A. *J. Am. Chem. Soc.* **2000**, *122*, 5147−5157. (b) Khaorapapong, N.; Ogawa, M. *Appl. Clay Sci.* **2007**, *35*, 31−38.
(24) (a) Nelson, J. C.; Saven, J. G.; Moore, J. S.; Wolynes, P. G. *Science* **1997**, *277*, 1793−1796. (b) Bloomfield, V. A.; Crothers, D. M.; Tinoco, I. *Physical Chemistry of Nucleic Acids*; Harper & Row: New York, 1974. (c) Cantor, C. R.; Schimmel, P. R. *Biophysical Chemistry*; Freeman: New York, 1980.
(25) (a) Fuller, A. A.; Seidl, F. J.; Bruno, P. A.; Plescia, M. A.; Palla, K. S. *Pept. Sci.* **2011**, *96*, 627−638. (b) Eftink, M. R.; Ghiron, C. A. *Biochemistry* **1976**, *15*, 672−680.
(26) Wojtuszewski, K.; Hawkins, M. E.; Cole, J. L.; Mukerji, I. *Biochemistry* **2001**, *40*, 2588−2598.
(27) (a) Hill, A. V. *Biochem. J.* **1913**, *7*, 471−480. (b) Byers, L. D. *J. Chem. Educ.* **1977**, *54*, 352−354.
(28) (a) Hunter, C. A.; Anderson, H. L. *Angew. Chem., Int. Ed.* **2009**, *48*, 7488−7499. (b) Rebek, J.; Costello, T.; Marshall, L.; Wattley, R.; Gadwood, R. C.; Onan, K. *J. Am. Chem. Soc.* **1985**, *107*, 7481−7487. (c) Taylor, P. N.; Anderson, H. L. *J. Am. Chem. Soc.* **1999**, *121*, 11538−11545.
(29) Bronson, R. T.; Bradshaw, J. S.; Savage, P. B.; Fuangswasdi, S.; Lee, S. C.; Krakowiak, K. E.; Izatt, R. M. *J. Org. Chem.* **2001**, *66*, 4752−4758.